*J. Biochem.* **144,** 215–221 (2008)
doi:10.1093/jb/mvn058

# NMR Studies on the Equilibrium Unfolding of Ketosteroid Isomerase by Urea

**Hyeong Ju Lee[1,*], Do Soo Jang[2,*,†], Hyung Jin Cha[2], Hye Seon Moon[1], Bee Hak Hong[2], Kwan Yong Choi[2,§] and Hee Cheon Lee[1,‡]**

*[1]Department of Chemistry; and [2]Division of Molecular Life Sciences, Pohang University of Science and Technology, Pohang, Republic of Korea, 790-784*

Received February 26, 2008; accepted April 17, 2008; published online April 27, 2008

**Multidimensional NMR was employed to investigate the structural changes in the urea-induced equilibrium unfolding of the dimeric ketosteroid isomerase (KSI) from *Pseudomonas putida* biotype B. Sequence specific backbone assignments for the native KSI and the protein with 3.5 M urea were carried out using various 3D NMR experiments. Hydrogen exchange measurements indicated that the secondary structures of KSI were not affected significantly by urea up to 3.5 M. However, the chemical shift analysis of $^{1}H$-$^{15}N$ HSQC spectra at various urea concentrations revealed that the residues in the dimeric interface region, particularly around the β5-strand, were significantly perturbed by urea at low concentrations, while the line-width analysis indicated the possibility of conformational exchange at the interface region around the β6-strand. The results thus suggest that the interface region primarily around the β5- and β6-strands could play an important role as the starting positions in the unfolding process of KSI.**

**Key words: dimeric protein, equilibrium unfolding, ketosteroid isomerase, NMR, urea.**

Abbreviations: CD, circular dichroism; KSI, ketosteroid isomerase; HX, hydrogen exchange; HSQC, heteronuclear single quantum coherence; NMR, nuclear magnetic resonance.

Protein folding is an active and important research area in current structural biology (*1*), and extensive studies on the folding pathways for a number of proteins have been performed by various experimental or theoretical methods. However, many of the studies have focused on the folding of monomeric proteins for simplicity, even though the self-association of proteins to form oligomers is a very common phenomenon and key factor in the regulation of proteins (*2*, *3*). Equilibrium unfolding is one of the useful methods for the study of protein folding and can provide definite insights into protein stabilities and structural changes during unfolding of proteins. Thus, circular dichroism (CD) and fluorescence spectroscopy have been extensively used to understand the global features of unfolding, in particular for the oligomeric proteins (*4*–*8*), while multidimensional nuclear magnetic resonance (NMR) has been used to obtain the unfolding characteristics at residue level (*9*–*14*).

Dimeric proteins take a large portion of oligomeric proteins and are largely distributed in living organisms (*15*). Their functionality is highly dependent on quaternary structures since their biological activity is often lost when the monomers separate from each other while most homodimeric proteins are composed of identical subunits each containing an active site (*2*). Ketosteroid isomerase (KSI) is a small homodimeric protein with six-stranded β-sheets and three α-helices in each cone-shaped monomer (Fig. 1), which catalyzes the isomerization of a wide variety of $\Delta^5$-3-ketosteroid to $\Delta^4$-3-ketosteroid by intramolecular transfer of the C4β proton to the C6β position (*16*). Homologous enzymes with 125 or 131 amino acid residues per monomer from two different bacterial sources, *Comamonas testosteroni* (previously known as *Pseudomonas testosteroni*) and *Pseudomonas putida* biotype B, have been extensively studied (*17*, *18*). Previous equilibrium unfolding studies by CD and fluorescence spectroscopy revealed that both forms of KSI followed a simple two-state folding mechanism (*19*, *20*). However, recent equilibrium unfolding studies on KSI from *P. putida* biotype B by other techniques such as small angle X-ray scattering and NMR self-diffusion measurement using pulsed-field gradient consistently indicated the existence of a distinct intermediate during unfolding (*21*).

In this study, we present multidimensional NMR investigations of the structural changes in the early stage of urea-induced equilibrium unfolding of KSI from *P. putida* biotype B. Sequence specific backbone assignments for the native KSI and the protein with 3.5 M urea were carried out using various 3D NMR experiments. The hydrogen exchange (HX) measurements as well as the chemical shift change and line-shape analyses of $^{1}H$-$^{15}N$ heteronuclear single quantum coherence (HSQC) spectra were performed for KSI at various urea

*These two authors contributed equally to this work.
†Present address: The J. David Gladstone Institute, SF, CA94158, USA.
‡To whom correspondence should be addressed. Tel: 82-54-279-2116, Fax: 82-54-279-3399, E-mail: hcl@postech.ac.kr
§Correspondence may also be addressed. Tel: 82-54-279-2295, Fax: 82-54-279-2199, E-mail: kchoi@postech.ac.kr

 

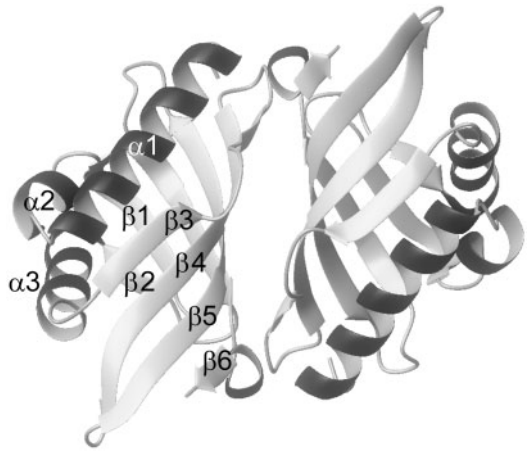


Fig. 1. **Crystal structure of dimeric KSI viewed roughly along the molecular 2-fold axis.**

concentrations up to 3.5 M. The urea concentrations of lower than 3.5 M were selected to investigate the subtle changes in the early stage of unfolding, since the global features of KSI have been shown to be almost identical below 4 M urea from the previous urea-induced unfolding studies of KSI (*21*). The results suggest that the unfolding of KSI might begin at the dimeric interface region primarily around the β5- and β6-strands, where the interactions are weakened first in the unfolding process by denaturant.

## MATERIALS AND METHODS

*Preparation of Labelled KSI Samples*—Uniformly $^{15}N$ labelled KSI was purified from *Escherichia coli* BL21 DE3 (Novagen Inc.) grown in 2 l of minimal medium (M9) containing $^{15}N$ ammonium chloride as the nitrogen source. The $^{13}C$-, $^{15}N$- and $^{2}H$ labelled protein sample was over expressed in the M9 medium containing $^{13}C$ glucose, $^{15}N$ ammonium chloride and $D_2O$, and purified as previously described (*19*). Homogeneity of KSI was confirmed by a single band in the PAGE analysis. $^{15}N$-labelled or triple-labelled KSI of ca. 1 mM was dissolved in 20 mM potassium phosphate buffer (pH 7.0, 10% v/v $D_2O$) with 1 mM dithiothreitol (DTT) and a small amount of sodium 2,2-dimethyl-2-silapentane-5-sulphonate (DSS) for internal chemical shift reference. Protein solutions at various urea concentrations were prepared by dissolving KSI in the phosphate buffer described above with appropriate amounts of urea and left at room temperature for 48 h to reach equilibrium.

*NMR Measurements and Backbone Assignments*—NMR experiments for backbone assignments were performed at 298 K on a Bruker Avance 800 spectrometer (800.25 MHz for $^{1}H$ frequency; Korea Basic Science Institute at Ochang) equipped with a triple resonance probe and pulsed field *x*-, *y*-, *z*-gradient capabilities. Sequence specific backbone assignments were obtained from the triple resonance experiments, HNCA, HN(CO)CA, HNCACB and HN(CO)CACB in TROSY type. HNCA and HN(CO)CA spectra were recorded with 70 data points along $t_1$ domain with a width of 6,840 Hz, 48 data points along $t_2$ domain with a width of 2,600 Hz and 1,024 data points along $t_3$ domain with a spectral width of 9,620 Hz. HNCACB and HN(CO)CACB spectra were recorded with 122 data points along $t_1$ domain with a width of 13,280 Hz, 48 data points along $t_2$ domain with a width of 2,600 Hz and 1,024 data points along $t_3$ domain with a spectral width of 9,620 Hz. All 3D NMR spectra were recorded using Echo-Antiecho method (*22*) in $t_2$ dimension and States-TPPI method (*23*) in $t_1$ dimension with a relaxation delay of 1 s.

2D NMR experiments were performed at 298 K on a Bruker DRX 500 spectrometer (500.13 MHz for $^{1}H$ frequency) equipped with a broad-band inverse probe and pulsed-field *z*-gradient capability. $^{1}H$-$^{15}N$ TROSY-HSQC spectra were recorded with 256 data points along $t_1$ domain with a width of 2,030 Hz and 4,096 complex data points along $t_2$ domain with a spectral width of 7,000 Hz using States-TPPI method in $t_1$ dimension with a relaxation delay of 1 s. All data sets were processed with NMRPipe (*24*), and analysed by Sparky (*25*) and MARS (*26*) to assign the resonances along the primary sequence of KSI. The $^{1}H$ chemical shifts were calibrated to DSS, and indirect referencing was used for the determination of $^{15}N$ chemical shifts (*27*).

*HX Measurements*—KSI solution of 100 μl in potassium phosphate buffer (pH 7.0, 100% $H_2O$) with an appropriate amount of urea was mixed with 400 μl $D_2O$ solution with the same salt, pH and urea conditions. This protein sample was mixed vigorously for 1–2 min using a vortex machine, centrifuged for ca. 20 s to remove air bubbles and then transferred to the probe for NMR experiments. The dead time for HX experiment was about 30 min due to relatively long preparation process including the $D_2O$ mixing, temperature adjustment, probe tuning and magnet shimming.

A series of $^{1}H$-$^{15}N$ TROSY-HSQC spectra were recorded for ~24 h to obtain the HX rates of amide protons. Each HSQC spectrum was recorded with 128 data points along $t_1$ domain and 2,048 complex data points along $t_2$ domain using States-TPPI method in $t_1$ dimension with a relaxation delay of 1 s. Scans of 16 were collected at each point along $t_1$ domain, and each HSQC spectrum took about 40 min to be recorded. The decrease in the peak intensity of each residue with time was fitted to single-ex ponential kinetics as given by (*28*):

$$I(t) = (I_0 - I_\infty)\exp(-k_{ex}t) + I_\infty \quad (1)$$

where $I_0$ is the intensity at time zero, $I_\infty$ the intensity at time infinity, and $k_{ex}$ the observed HX rate constant. Since the dead time of 30 min for the HX experiment is relatively long, any residues having the HX rates faster than the dead time cannot be probed in this study. In order to correlate the HX rates with protecting structures quantitatively, the protection factor ($P$) was calculated according to the following equation (*29*):

$$P = \frac{k_i}{k_{obs}} \quad (2)$$

where $k_i$ and $k_{obs}$ are the intrinsic HX rate constant in polypeptide chain (*30*) and the measured one from KSI, respectively.

## RESULTS AND DISCUSSION

Sequence specific backbone assignments were carried out using the characteristic chemical shifts of the $^{13}C^{\alpha}$ of 13 glycines in HNCA spectra, $^{13}C^{\beta}$ of 12 alanines, 3 serines, 4 theronines and 180 phase-shifted $^{13}C^{\alpha}$ of 13 glycines in HNCACB spectra as starting points (*31*) as well as the general characteristics of HNCA and HNCACB experiments. A total of 110 and 107 residues were assigned for the native KSI (without urea) and the protein with 3.5 M urea, respectively. Figure 2 shows the finger print $^{1}H$-$^{15}N$ HSQC spectrum of the native KSI, and the HSQC spectrum of KSI with 3.5 M urea was very similar to that of the native KSI. (See the Supplementary Data for $^{1}H$ and $^{15}N$ chemical shifts.)

The HX experiment has been widely used in the NMR studies of protein folding because it can provide information about the presence or absence of protecting structures at amino acid resolution (*32*, *33*). The HX rate for each of the amino acid residues of KSI was measured at both native (0 M urea) and 3.5 M urea conditions, and the protection factors ($P$) were estimated by Eq. (2) using the observed HX rates. Two features can be easily seen in Fig. 3A and B, where the $P$-values for the native KSI and the protein with 3.5 M urea are expressed in log scale. Firstly, the protection factors vary significantly with the positions of residues in protein. Roughly, the residues located at α3-helix, β3-strand and adjacent to N- and C-terminal exhibit lower protection factors than those in other secondary structure elements. In fact, the HX rates for many of the residues in these secondary structure elements were too fast to be detected experimentally with the dead time of about 30 min even at the native condition. As a result, the HX rates of only 53 relatively well-protected amino acid residues were properly measured, while the protection factors for the undetectably fast residues were set to an arbitrary number (log $P = 2$ in Fig. 3). Figure 3C shows the solvent accessible surface areas (SASA) for the backbone amides of KSI (*34*).

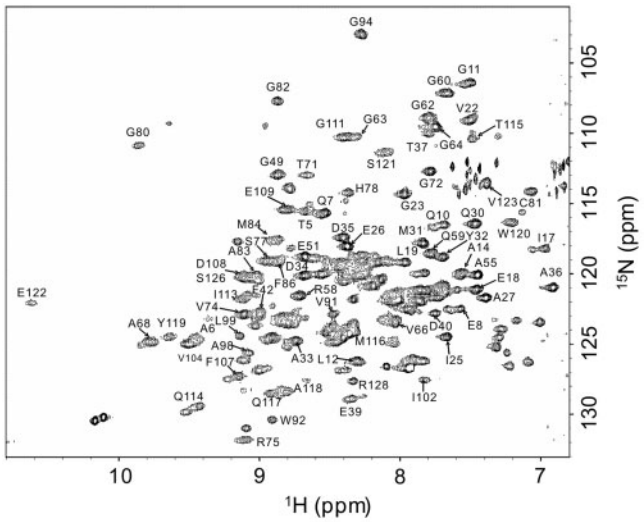


Fig. 2. **Fingerprint $^{1}H$-$^{15}N$ HSQC spectrum of the native KSI. Some of the labels are not shown because of severe overlaps between resonances.**

As might be expected, a comparison between Fig. 3A (or B) and C shows that there is a close correlation between the protection factor and SASA, where the residues with large backbone SASA are less protected from the solvent than those with small SASA. Secondly, the protection factors for most of the 53 residues decrease almost uniformly with faster exchange rates as the urea concentration increases from 0 to 3.5 M, while there are no meaningful differences in the urea-induced change of protection factor between the residues. Since the protection factor can be related to structural characteristics of protein including the extent of solvent exposure (*35*), the result implies that the secondary (or tertiary) structures of KSI are not affected significantly by 3.5 M urea, though there could be an uniform increase in the rate of backbone fluctuation as a result of the decreased thermodynamic stability of protein at higher urea concentrations. This result is consistent with

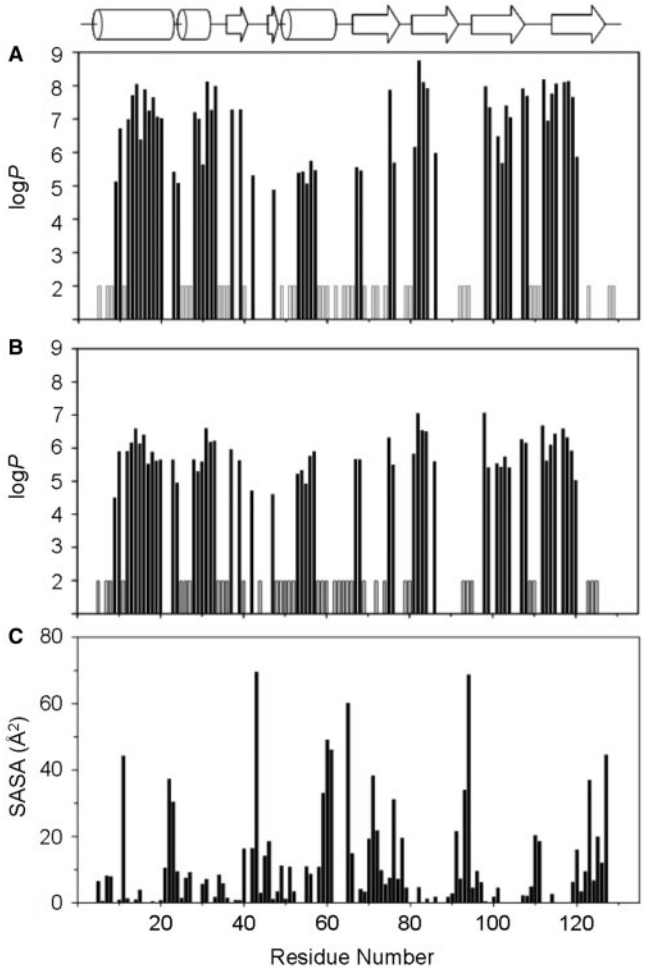


Fig. 3. **Plots of the protection factors as a function of residue number for KSI at 0 M (A) and 3.5 M (B) urea conditions.** The protection factors were calculated by Eq. (2) using the observed HX rates. The residues having undetectably fast exchange rates are represented by light gray bars, whose values are set to an arbitrary number (log $P = 2$). (C) Plot of the solvent accessible surface areas for the backbone amides of KSI as a function of residue number.

those of previous equilibrium unfolding experiments using CD and fluorescence spectroscopy that the secondary structures of KSI were not significantly altered by urea up to the concentration of 4 M (*19*).

The peak positions of a majority of the residues in $^{1}$H-$^{15}$N HSQC spectra at 0 and 3.5 M urea conditions were very similar in overall. However, some of the resonances showed small, but distinct differences in the shifts at the two urea conditions, which could be attributed to the local perturbations in the structural characteristics of KSI by urea. In order to further investigate the local structural perturbations, $^{1}$H-$^{15}$N HSQC spectra were collected from the KSI samples at various urea concentrations of 0, 0.5, 1.0, 2.0, 3.0 and 3.5 M. Resonance assignments for KSI at 0.5, 1.0, 2.0 and 3.0 M urea conditions were achieved by a comparison of the observed $^{1}$H-$^{15}$N HSQC spectra with those of KSI at 0 and 3.5 M urea conditions, which have been fully assigned by 3D NMR experiments. Figure 4 shows the representative $^{1}$H-$^{15}$N HSQC spectra of KSI at 0.5 and 3.5 M urea conditions. While the spectra look very similar each other, the peak intensities of three resonances from Trp120, Glu122 and Val123 residues are significantly reduced with the increase in urea concentration. Figure 5A shows the plot of the $^{1}$H line-widths as a function of residue number at 3.5 M urea condition, where the residues with the line-widths of greater than the average (ca. 30 Hz) appear to be localized in the regions around the β5- and β6-strands. When the line-widths of the residues were normalized to the corresponding values of native KSI (0 M urea condition) for comparison, the three residues Trp120, Glu122 and Val123 were found to have the largest normalized line-widths. Figure 5B shows the plot of the normalized $^{1}$H line-widths for these residues as a function of urea concentration. As can be seen in Fig. 5B, the normalized $^{1}$H line-widths for the three residues are gradually increased with the increase in urea concentration, while the average value for all the other residues remains almost the same at all urea concentrations.

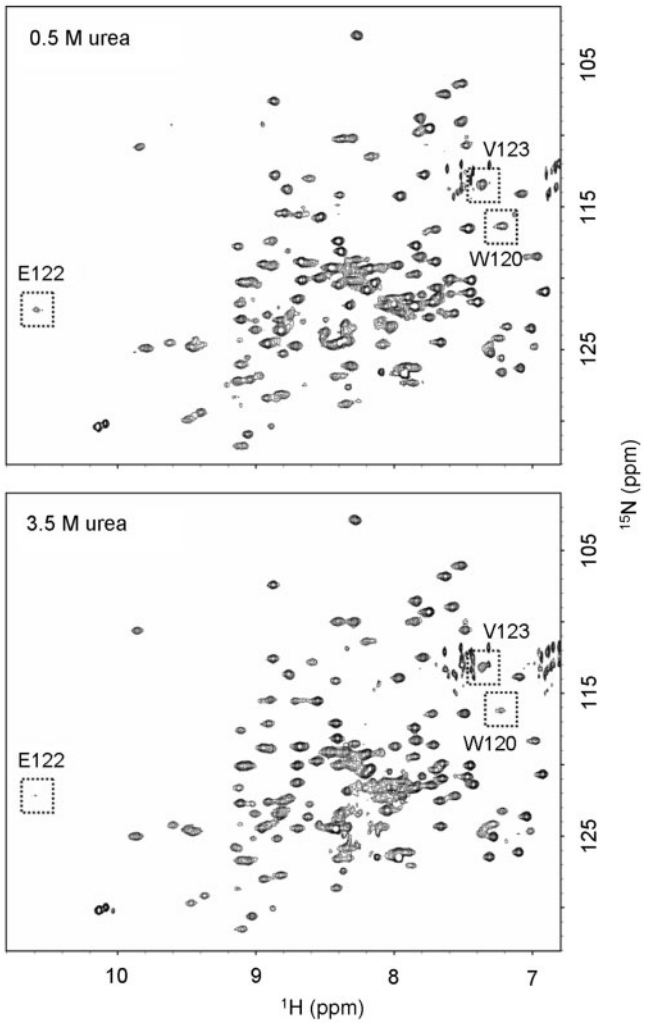


Fig. 4. **Representative $^{1}$H-$^{15}$N HSQC spectra of KSI at the urea concentrations of 0.5 and 3.5 M.** Intensities of the three boxed residues (Trp120, Glu122 and Val123) are significantly reduced with the increase in urea concentration.

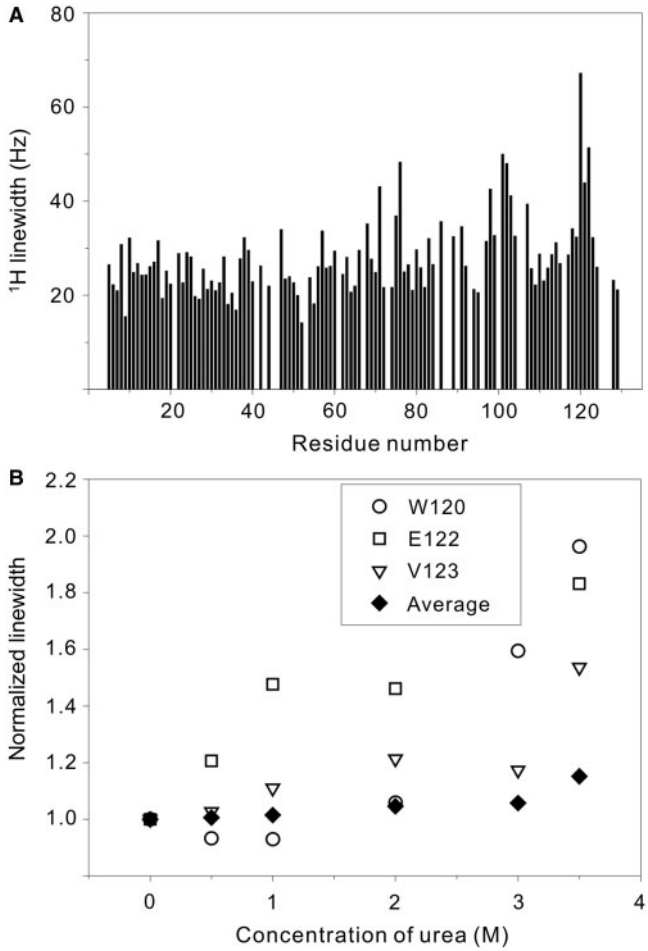


Fig. 5. **Plots of (A) the $^{1}$H line-widths as a function of residue number at 3.5 M urea condition and (B) the line-widths for Trp120, Glu122 and Val123 as a function of urea concentration.** The line-widths at each urea concentration were normalized to the corresponding values of native KSI (0 M urea condition). The 'Average' represents the average value of normalized line-widths for all the other residues of KSI.

In general, the line-width will increase if there exists a chemical or conformational exchange between two different sites with a slow exchange rate on NMR time scale, and the rate becomes faster due to enhanced overall or internal motions. In the case of KSI unfolding by urea, the backbone fluctuations seem to be enhanced at higher urea concentrations as evidenced by the results of HX experiments (Fig. 3). Then, the increased line-widths at higher urea concentrations may suggest that there exists a moderately fast exchange between two conformers of well-structured dimeric KSI, particularly in the region around the three residues. The results of our previous study on the size of KSI during urea-induced unfolding by diffusion NMR and small angle X-ray scattering measurements indicated that KSI exists as a compact monomer-like intermediate at the urea condition of 5.2 M, while the protein maintains the dimeric form below 4.0 M urea (*21*). Interestingly, the three residues compose a β-bulge structure in the β6-strand of KSI and also participate in the formation of dimeric interface (*36*). Such a conformational exchange between two protein conformers has also been observed in other proteins such as SUMO-1 (*10*) and DLC8 (*37*).

In order to investigate the local structural perturbations of KSI by urea in detail at residue level, the cumulative chemical shift changes ($\Delta\delta_{cum}$) were calculated for each of the residues according to the following equation (*38*):

$$\Delta\delta_{cum} = \left[(\Delta\delta_N)^2 + (\Delta\delta_H)^2\right]^{1/2} \quad (3)$$

where $\Delta\delta_N$ and $\Delta\delta_H$ denote the urea-induced chemical shift changes at various urea concentrations measured in Hz in the $^1H$ and $^{15}N$ dimensions, respectively. The $\Delta\delta_{cum}$ values were quite small for most of the residues at all urea concentrations, however, many of the residues exhibited distinct dependence of $\Delta\delta_{cum}$ on the urea concentration. Thus, the $\Delta\delta_{cum}$ values for some residues were quite large even at 0.5 M urea condition with little dependence on the urea concentration, while other residues showed linear correlations between $\Delta\delta_{cum}$ and the urea concentration with relatively small $\Delta\delta_{cum}$ at 0.5 M urea condition (data not shown), indicating that the local structural perturbations are quite different along the sequence.

Figure 6 shows the plots of $\Delta\delta_{cum}$ as a function of residue number for KSI at 0.5 and 3.5 M urea conditions, which represent the relatively early and midway stages of urea-induced unfolding process. The residues that have relatively large $\Delta\delta_{cum}$ over a specific cut off (a sum of the average and standard deviation of $\Delta\delta_{cum}$) at each urea concentration are labelled on the histogram and marked by black on the ribbon diagram of native structure of KSI besides the plots. As expected, the $\Delta\delta_{cum}$ values at 3.5 M urea condition are much larger than those at 0.5 M urea condition, indicating significantly enhanced structural perturbations at higher urea concentrations. More specifically, a total of 10 residues such as Arg15, Phe42, Ile47, His48, Thr71, Ala76, Asp103, Val104, Met105 and Ser121 show relatively large $\triangle\delta_{cum}$ over the cut off of ca. 20 Hz at 0.5 M urea condition (Fig. 6A). Interestingly, six of the 10 residues (Phe42, Ala76, Asp103, Val104, Met105 and Ser121) are located at the dimeric interface region, and three of the 6 interface residues (Asp103, Val104, Met105) belong to the β5-strand. This observation indicates that the dimeric interface region, particularly the β5-strand could be significantly perturbed by denaturant such as

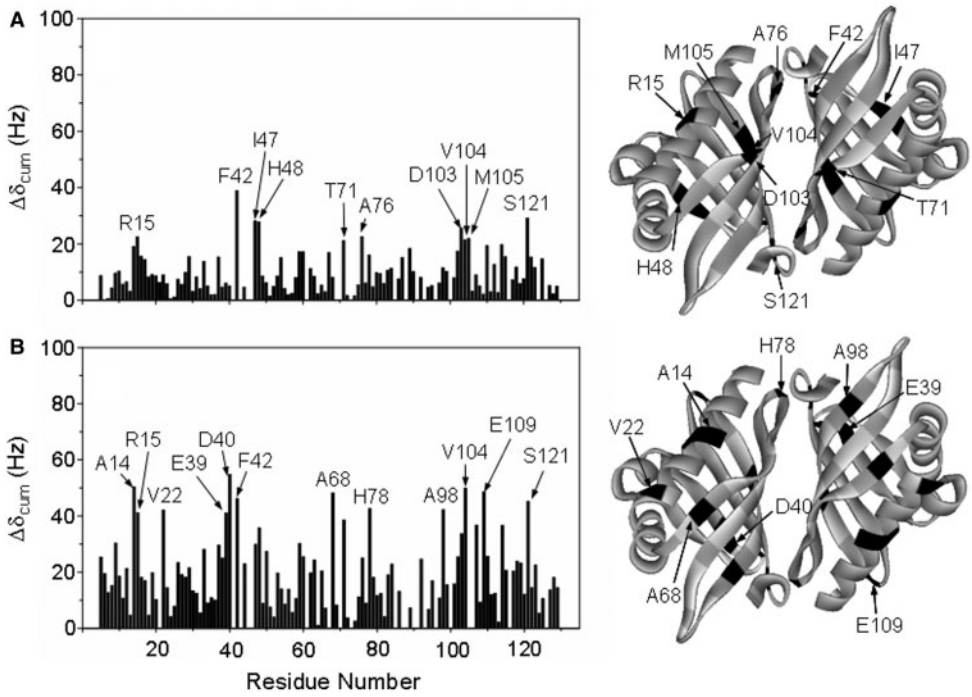


Fig. 6. **Plots of the $\Delta\delta_{cum}$ as a function of residue number for KSI at 0.5 M (A) and 3.5 M (B) urea conditions.** Changes beyond a specific cut off (see text) are marked by black on the ribbon diagram of native structure of KSI besides the plots. The residues for which the $\triangle\delta_{cum}$ could not be determined due to lack of measured data are marked by white.

urea even at very low concentrations. On the other hand, a total of 12 residues such as Ala14, Arg15, Val22, Glu39, Asp40, Phe42, Ala68, His78, Ala98, Val104, Glu109 and Ser121 show large $\triangle\delta_{cum}$ over the cut off of ca. 40 Hz at 3.5 M urea condition (Fig. 6B). However, only four of the 12 residues (Phe42, His78, Val104 and Ser121) are located at the dimeric interface region, indicating that the structural perturbations are not localized any longer in the dimeric interface region, particularly around β5-strand at 3.5 M urea. Two clusters can be noticeable around the regions of 39–48 and 92–121 residues in Fig. 6B, where the former cluster mainly corresponds to a flexible loop, while the latter one is comprised of β5- and β6-strands. The results of chemical shift analyses thus suggest that the structural perturbations are initially localized in the dimeric interface region around β5-strand at low urea condition and would spread all over the protein including the entire interface region in the midway of unfolding, which could lead to dissociation of dimeric KSI into structured monomers at higher denaturant concentrations as the interactions in the interface region are weakened or collapsed. Similar observation has also been reported in the mass spectrometric study on the unfolding of creatine kinase (CK) induced by GdmHCl of $\leq$0.8 M, where the regions involved in the dimeric interface of CK were very sensitive to low GdmHCl concentration (*39*).

In summary, we have investigated the effect of urea on the structural changes in the early stage of equilibrium unfolding of KSI by using various multidimensional NMR techniques. HX measurements indicated that no remarkable changes occurred in the secondary (or tertiary) structures of KSI up to the urea concentration of 3.5 M. However, the chemical shift analysis of $^{1}H$-$^{15}N$ HSQC spectra at various urea concentrations revealed that the residues in the dimeric interface region, particularly around the β5-strand, were significantly perturbed by urea at low concentrations, while the linewidth analysis indicated the possibility of conformational exchange at the dimeric interface region, particularly around the β6-strand. Taken together, it can be concluded that the dimeric interface region primarily around the β5- and β6-strands would be perturbed first by urea in the early stage of unfolding, and the unfolding of KSI might begin at this interface region of two strands.

Supplementary data are available at *JB* Online.

This work was supported by the grant from Korea Research Foundation (C00178).

REFERENCES

1. Miranker, A.D. and Dobson, C.M. (1996) Collapse and cooperativity in protein folding. *Curr. Opin. Struct. Biol.* **6**, 31–42
2. Mei, G., Di Venere, A., Rosato, N., and Finazzi-Agro, A. (2005) The importance of being dimeric. *FEBS J.* **272**, 16–27
3. de Prat-Gay, G., Nadra, A.D., Corrales-Izquierdo, F.J., Alonso, L.G., Ferreiro, D.U., and Mok, Y.K. (2005) The folding mechanism of a dimeric β-barrel domain. *J. Mol. Biol.* **351**, 672–682
4. Mallam, A.L. and Jackson, S.E. (2006) Probing nature's knots: the folding pathway of a knotted homodimeric protein. *J. Mol. Biol.* **359**, 1420–1436
5. Talbott, M., Hare, M., Nyarko, A., Hays, T.S., and Barbar, E. (2006) Folding is coupled to dimerization of Tctex-1 dynein light chain. *Biochemistry* **45**, 6793–6800
6. Horng, J.C., Tracz, S.M., Lumb, K.J., and Raleigh, D.P. (2005) Slow folding of a three-helix protein via a compact intermediate. *Biochemistry* **44**, 627–634
7. Chedad, A. and Van Dael, H. (2004) Kinetics of folding and unfolding of goat alpha-lactalbumin. *Proteins* **57**, 345–356
8. Martins, S.M., Chapeaurouge, A., and Ferreira, S.T. (2002) Equilibrium unfolding and conformational plasticity of troponin I and T. *Eur. J. Biochem.* **269**, 5484–5491
9. Kitahara, R., Yamaguchi, Y., Sakata, E., Kasuya, T., Tanaka, K., Kato, K., Yokoyama, S., and Akasaka, K. (2006) Evolutionally conserved intermediates between ubiquitin and NEDD8. *J. Mol. Biol.* **363**, 395–404
10. Kumar, A., Srivastava, S., Kumar Mishra, R., Mittal, R., and Hosur, R.V. (2006) Residue-level NMR view of the urea-driven equilibrium folding transition of SUMO-1 (1-97): native preferences do not increase monotonously. *J. Mol. Biol.* **361**, 180–194
11. Korzhnev, D.M., Bezsonova, I., Evanics, F., Taulier, N., Zhou, Z., Bai, Y., Chalikian, T.V., Prosser, R.S., and Kay, L.E. (2006) Probing the transition state ensemble of a protein folding reaction by pressure-dependent NMR relaxation dispersion. *J. Am. Chem. Soc.* **128**, 5262–5269
12. Tang, Y., Grey, M.J., McKnight, J., Palmer, , A.G. 3rd, , and Raleigh, D.P. (2006) Multistate folding of the villin headpiece domain. *J. Mol. Biol.* **355**, 1066–1077
13. Casares, S., Sadqi, M., Lopez-Mayorga, O., Conejero-Lara, F., and van Nuland, N.A. (2004) Detection and characterization of partially unfolded oligomers of the SH3 domain of alpha-spectrin. *Biophys. J.* **86**, 2403–2413
14. Li, H. and Frieden, C. (2005) Phenylalanine side chain behavior of the intestinal fatty acid-binding protein: the effect of urea on backbone and side chain stability. *J. Biol. Chem.* **280**, 38556–38561
15. Nicolai, E., Di Venere, A., Rosato, N., Rossi, A., Finazzi Agro, A., and Mei, G. (2006) Physico-chemical properties of molten dimer ascorbate oxidase. *FEBS J.* **273**, 5194–5204
16. Pollack, R.M. (2004) Enzymatic mechanisms for catalysis of enolization: ketosteroid isomerase. *Bioorg. Chem.* **32**, 341–353
17. Ha, N.C., Choi, G., Choi, K.Y., and Oh, B.H. (2001) Structure and enzymology of $\triangle^{5}$-3-ketosteroid isomerase. *Curr. Opin. Struct. Biol.* **11**, 674–678
18. Pollack, R.M., Thornburg, L.D., Wu, Z.R., and Summers, M.F. (1999) Mechanistic insights from the three-dimensional structure of 3-oxo-$\triangle^{5}$-steroid isomerase. *Arch. Biochem. Biophys.* **370**, 9–15
19. Kim, D.H., Nam, G.H., Jang, D.S., Yun, S., Choi, G., Lee, H.C., and Choi, K.Y. (2001) Roles of dimerization in folding and stability of ketosteroid isomerase from *Pseudomonas putida* biotype B. *Protein Sci.* **10**, 741–752
20. Kim, D.H., Jang, D.S., Nam, G.H., Yun, S., Cho, J.H., Choi, G., Lee, H.C., and Choi, K.Y. (2000) Equilibrium and kinetic analysis of folding of ketosteroid isomerase from *Comamonas testosteroni*. *Biochemistry* **39**, 13084–13092
21. Jang, D.S., Lee, H.J., Lee, B., Hong, B.H., Cha, H.J., Yoon, J., Lim, K., Yoon, Y.J., Kim, J., Ree, M., Lee, H.C., and Choi, K.Y. (2006) Detection of an intermediate during the unfolding process of the dimeric ketosteroid isomerase. *FEBS Lett.* **580**, 4166–4171
22. Kay, L.E., Keifer, P., and Saarinen, T. (1992) Pure absorption gradient enhanced heteronuclear single quantum correlation spectroscopy with improved sensitivity. *J. Am. Chem. Soc.* **114**, 10663–10665
23. Marion, D., Driscoll, P.C., Kay, L.E., Wingfield, P.T., Bax, A., Gronenborn, A.M., and Clore, G.M. (1989) Overcoming the overlap problem in the assignment of $^{1}H$ NMR spectra of

larger proteins by use of three-dimensional heteronuclear $^{1}H$-$^{15}N$ Hartmann-Hahn-multiple quantum coherence and nuclear Overhauser-multiple quantum coherence spectroscopy: application to interleukin 1β. *Biochemistry* **28**, 6150–6156
24. Delaglio, F., Grzesiek, S., Vuister, G.W., Zhu, G., Pfeifer, J., and Bax, A. (1995) NMRPipe: a multidimensional spectral processing system based on UNIX pipes. *J. Biomol. NMR* **6**, 277–293
25. Goddard, T.D. and Kneller, D.G. *Sparky3*. University of California, San Fransisco
26. Jung, Y.S. and Zweckstetter, M. (2004) Mars – robust automatic backbone assignment of proteins. *J. Biomol. NMR* **30**, 11–23
27. Wishart, D.S., Bigam, C.G., Yao, J., Abildgaard, F., Dyson, H.J., Oldfield, E., Markley, J.L., and Sykes, B.D. (1995) $^{1}H$, $^{13}C$ and $^{15}N$ chemical shift referencing in biomolecular NMR. *J. Biomol. NMR* **6**, 135–140
28. Mohs, A., Popiel, M., Li, Y., Baum, J., and Brodsky, B. (2006) Conformational features of a natural break in the type IV collagen Gly-X-Y repeat. *J. Biol. Chem.* **281**, 17197–17202
29. Finucane, M.D. and Jardetzky, O. (1996) The pH dependence of hydrogen-deuterium exchange in trp repressor: the exchange rate of amide protons in proteins reflects tertiary interactions, not only secondary structure. *Protein Sci.* **5**, 653–662
30. Bai, Y., Milne, J.S., Mayne, L., and Englander, S.W. (1993) Primary structure effects on peptide group hydrogen exchange. *Proteins* **17**, 75–86
31. Zhao, Q., Abeygunawardana, C., and Mildvan, A.S. (1997) NMR studies of the secondary structure in solution and the steroid binding site of $\triangle^{5}$-3-ketosteroid isomerase in complexes with diamagnetic and paramagnetic steroids. *Biochemistry* **36**, 3458–3472
32. Nishimura, C., Dyson, H.J., and Wright, P.E. (2006) Identification of native and non-native structure in kinetic folding intermediates of apomyoglobin. *J. Mol. Biol.* **355**, 139–156
33. Krishna, M.M., Hoang, L., Lin, Y., and Englander, S.W. (2004) Hydrogen exchange methods to study protein folding. *Methods* **34**, 51–64
34. Fraczkiewicz, R. and Braun, W. (1998) Exact and efficient analytical calculation of the accessible surface areas and their gradients for macromolecules. *J. Comp. Chem.* **19**, 319–333
35. Perrett, S., Clarke, J., Hounslow, A.M., and Fersht, A.R. (1995) Relationship between equilibrium amide proton exchange behavior and the folding pathway of barnase. *Biochemistry* **34**, 9288–9298
36. Kim, S.W., Cha, S.S., Cho, H.S., Kim, J.S., Ha, N.C., Cho, M.J., Joo, S., Kim, K.K., Choi, K.Y., and Oh, B.H. (1997) High-resolution crystal structures of $\triangle^{5}$-3-ketosteroid isomerase with and without a reaction intermediate analogue. *Biochemistry* **36**, 14030–14036
37. Chatterjee, A., Krishna Mohan, P.M., Prabhu, A., Ghosh-Roy, A., and Hosur, R.V. (2007) Equilibrium unfolding of DLC8 monomer by urea and guanidine hydrochloride: distinctive global and residue level features. *Biochimie.* **89**, 117–134
38. Gröger, C., Moglich, A., Pons, M., Koch, B., Hengstenberg, W., Kalbitzer, H.R., and Brunner, E. (2003) NMR-spectroscopic mapping of an engineered cavity in the I14A mutant of HPr from Staphylococcus carnosus using xenon. *J. Am. Chem. Soc.* **125**, 8726–8727
39. Mazon, H., Marcillat, O., Forest, E., and Vial, C. (2005) Denaturant sensitive regions in creatine kinase identified by hydrogen/deuterium exchange. *Rapid Commun. Mass Spectrom* **19**, 1461–1468